NANO MICRO small

Supporting Information

for *Small,* DOI: 10.1002/smll.202300163

An Electroactive and Self-Assembling Bio-Ink, based on Protein-Stabilized Nanoclusters and Graphene, for the Manufacture of Fully Inkjet-Printed Paper-Based Analytical Devices

Alessandro Silvestri, Silvia Vázquez-Díaz, Giuseppe Misia, Fabrizio Poletti, Rocío López-Domene, Valeri Pavlov, Chiara Zanardi, Aitziber L. Cortajarena,* and Maurizio Prato**

Supporting Information

An electroactive and self-assembling bio-ink, based on proteins-stabilized nanoclusters and graphene, for the manufacture of fully inkjet-printed paper-based analytical devices.

Alessandro Silvestri[†]*, *Silvia Vázquez-Díaz*[†], *Giuseppe Misia, Fabrizio Poletti, Rocío López Domene, Valery Pavlov, Chiara Zanardi, Aitziber Lopez Cortajarena*, *Maurizio Prato**

[†] These authors contributed equally.

Protein design

The engineered CTPR proteins were produced by the assembly of different designed repeat modules: wildtype module (W_1), C_{4His} (H_2) module (AHAWHNLGHAYLHQGDYNEXXEYYQKALELDPRS) and C_{4Cys} (C_2) module (ACAWYCLGCAYLCQGDYDEAIEYYQKALELDPRS).

$C6_{His16}$ and $C6_{Cys16}$ proteins were generated by the combination of CTPR6-$W_1(H_2)_4W_1$ and CTPR6-$W_1(C_2)_4W_1$ modules respectively. The identities of the generated CTPR proteins were verified by DNA sequencing (Stab Vida).

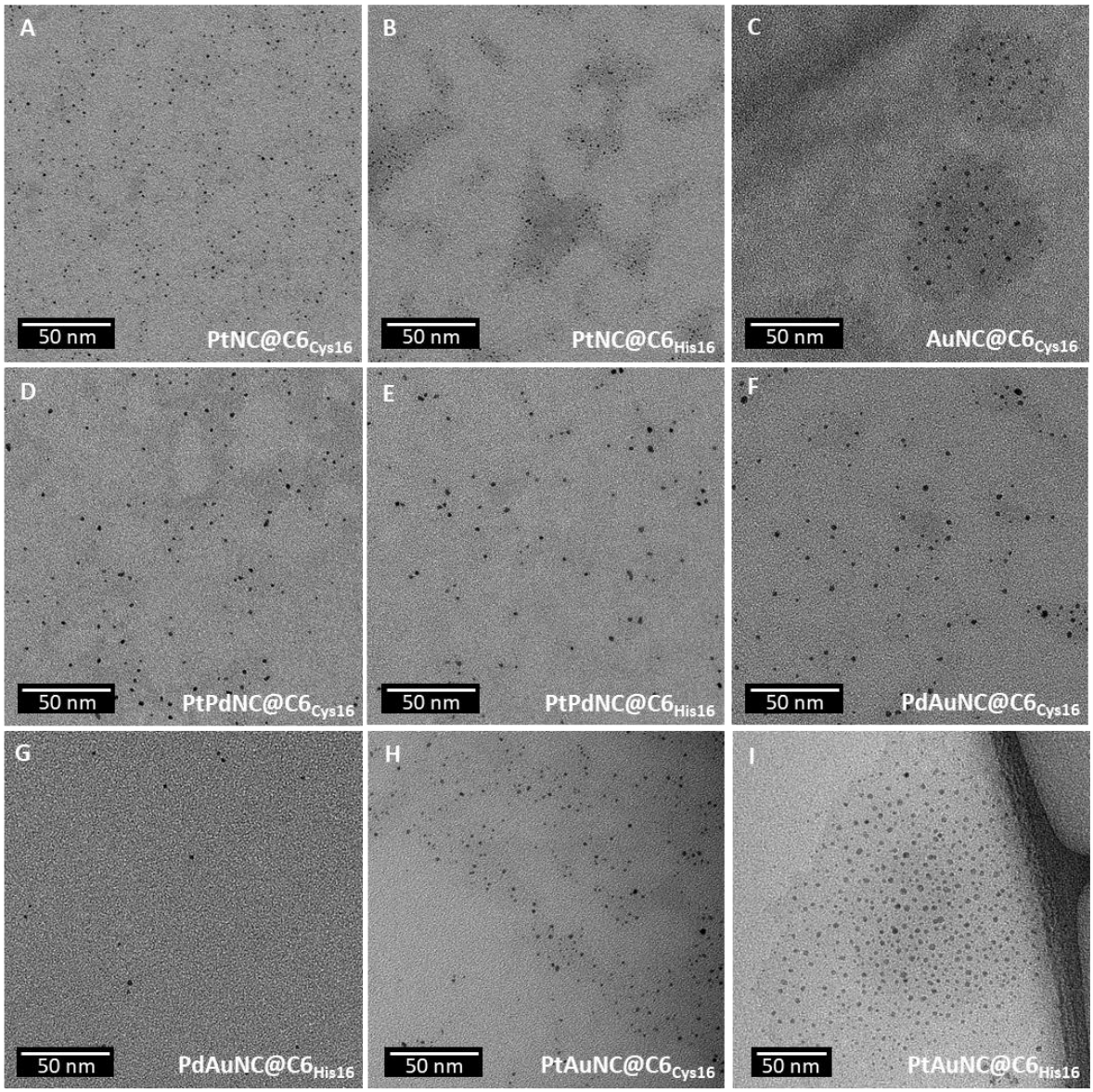

Figure S1. TEM micrographs of A) PtNC@C6$_{Cys16}$, B) PtNC@C6$_{His16}$, C) AuNC@C6$_{Cys16}$, D) PtPdNC@C6$_{Cys16}$, E) PtPdNC@C6$_{His16}$, F) PdAuNC@C6$_{Cys16}$, G) PdAuNC@C6$_{His16}$, H) PtAuNC@C6$_{Cys16}$, I) PtAuNC@C6$_{His16}$.

Table S1. Protein and metal concentration in the CTPR-NCs and their ratios.

NCs@C6	Nominal M1/M2 ratio	[CTPR]* (μM)	[M1]** (μM)	[M2]** (μM)	M1/CTPR	M2/CTPR	M1/M2
$PtAuNC@C6_{Cys16}$	10	9.70	739.17 ± 0.01	69.04 ± 1.56	76.19	7.11	10.71
$PtAuNC@C6_{His16}$	10	13.88	701.63 ± 8.05	101.32 ± 0.83	50.55	7.30	6.92
$PtNC@C6_{Cys16}$	-	15.45	375.91 ± 34.70	-	24.33	-	-
$PtNC@C6_{His16}$	-	19.70	405.50± 11.37	-	20.28	-	-
$AuNC@C6_{Cys16}$	-	30	154.01 ± 3.54	-	5.13	-	-
$PdAuNC@C6_{Cys16}$	10	36.3	951.79 ± 27.23	100.55 ± 4.43	26.22	2.77	9.46
$PdAuNC@C6_{His16}$	10	28.56	621.18 ± 155.37	38.76 ± 8.84	21.75	1.36	15.99
$PtPdNC@C6_{Cys16}$	1	43.52	799.46 ± 10.71	440.00 ± 5.31	18.37	10.11	1.82
$PtPdNC@C6_{His16}$	1	23.56	285.08 ± 8.25	267.17 ± 11.31	12.10	11.34	1.06

* Calculated from BCA measurements

** Calculated from ICP-MS measurements

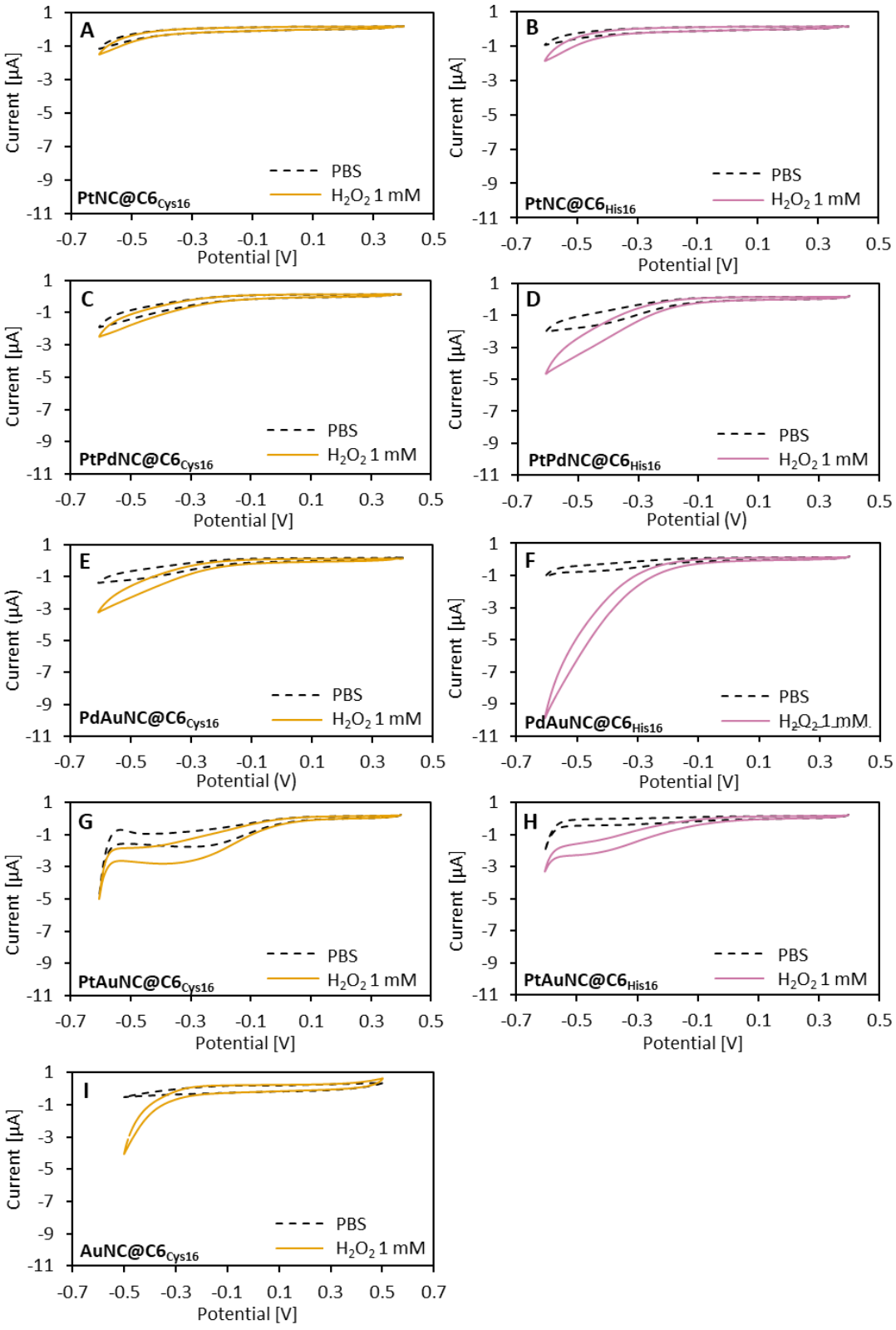

Figure S2. CV responses showing the cathodic currents generated by PtNC@C6$_{Cys16}$ (A), PtNC@C6$_{His16}$ (B), AuNC@C6$_{Cys16}$ (C), PtPdNC@C6$_{Cys16}$ (D), PtPdNC@C6$_{His16}$ (E), PdAuNC@C6$_{Cys16}$ (F), PdAuNC@C6$_{His16}$ (G), PtAuNC@C6$_{Cys16}$ (H), PtAuNC@C6$_{His16}$ (I) in presence (solid line) and in absence (dashed line) of 1 mM H_2O_2 (scan rate: 20 mV s^{-1}, electrolyte 0.1 M PBS 0.1 M KCl, WE: GC, CE: Pt mesh RE: Ag/AgCl, Argon atmosphere).

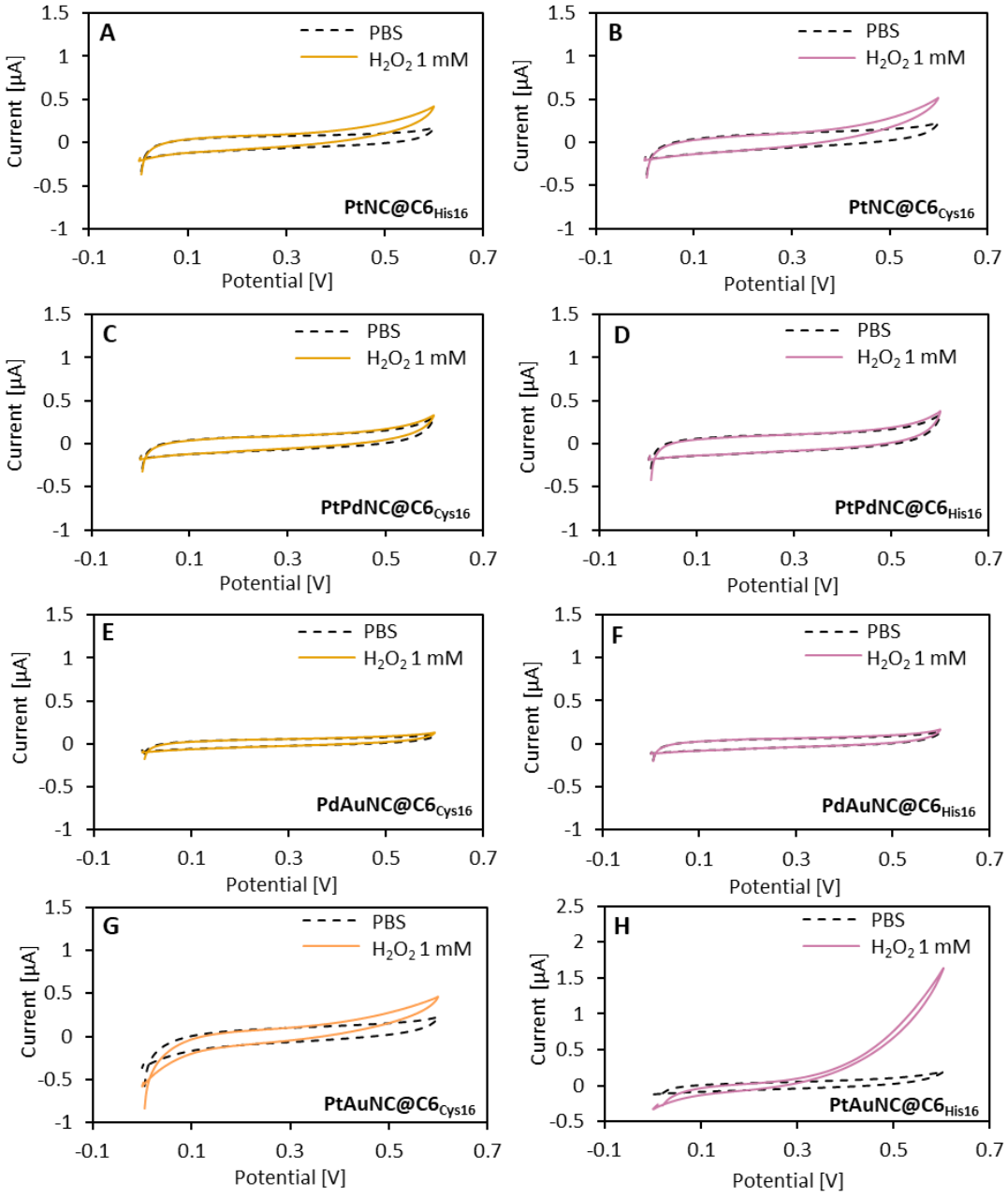

Figure S3. CV responses showing the anodic currents generated by PtNC@C6$_{Cys16}$ (A), PtNC@C6$_{His16}$ (B), AuNC@C6$_{Cys16}$ (C), PtPdNC@C6$_{Cys16}$ (D), PtPdNC@C6$_{His16}$ (E), PdAuNC@C6$_{Cys16}$ (F), PdAuNC@C6$_{His16}$ (G), PtAuNC@C6$_{Cys16}$ (H), in presence (solid line) and in absence (dashed line) of 1 mM H_2O_2 (scan rate: 20 mV s^{-1}, electrolyte 0.1 M PBS 0.1 M KCl, WE: GC, CE: Pt mesh RE: Ag/AgCl).

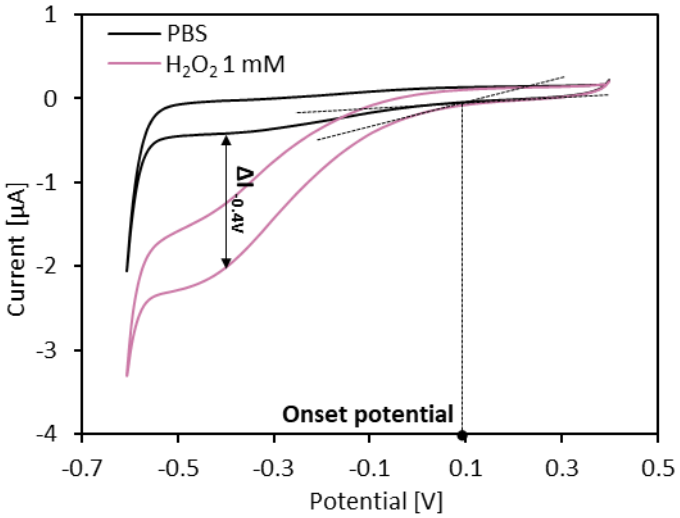

Figure S4. CV responses of PtAuNC@C6$_{His16}$ in presence and absence of 1 mM H_2O_2 (scan rate: 20 mV s^{-1}; electrolyte 0.1 M PBS and 0.1 M KCl; WE: GC; CE: Pt mesh; RE: Ag/AgCl). The onset potential has been calculated as the intercept between the draw tangents in non-faradaic and faradaic zones of the CV. The generated current was calculated as the difference of the currents registered at -0.4 V (in case of the cathodic current) and +0.4V (in case of the anodic current) in presence and in absence of 1 mM H_2O_2.

Table S2. Elemental composition of PtAuNC@C6$_{His16}$ obtained from the deconvolution of the XPS spectrum.

	Pt (0)		Pt (II)		Au (0)		Au (I)		C	O	N
	7/2	5/2	7/2	5/2	7/2	5/2	7/2	5/2			
B.E. (eV)	70.5	73.8	71.9	75.3	83.5	87.2	85.1	88.8	284.7	531.0	399.9
At %	5.29	4.05	2.92	1.65	0.38	0.38	0.23	0.18	51.63	23.88	2.9

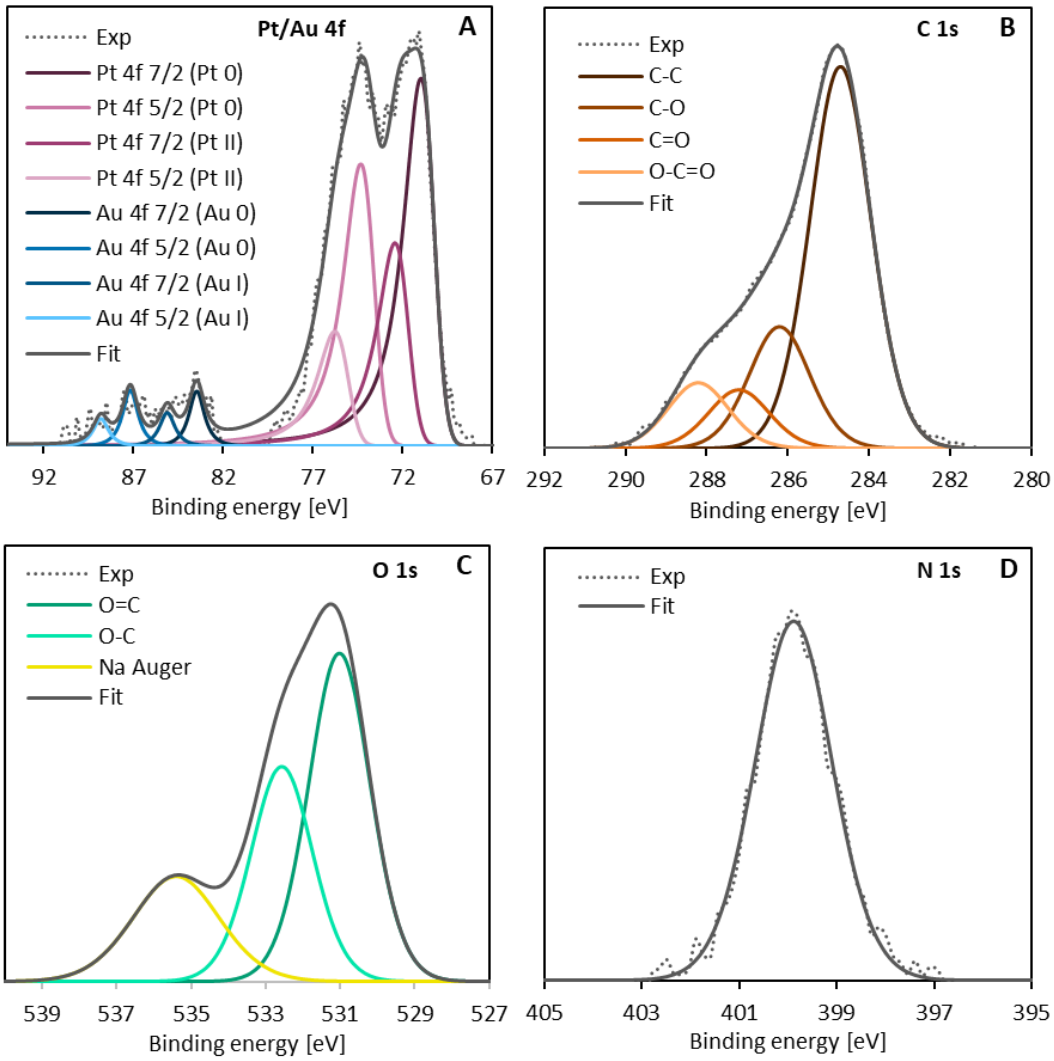

Figure S5. Deconvoluted high-resolution XPS spectra of the Au 4f and Pt 4f cores (A), C 1S core (B), O 1s core (C), and N 1s core (D) of PtAuNC@C6$_{His16}$.

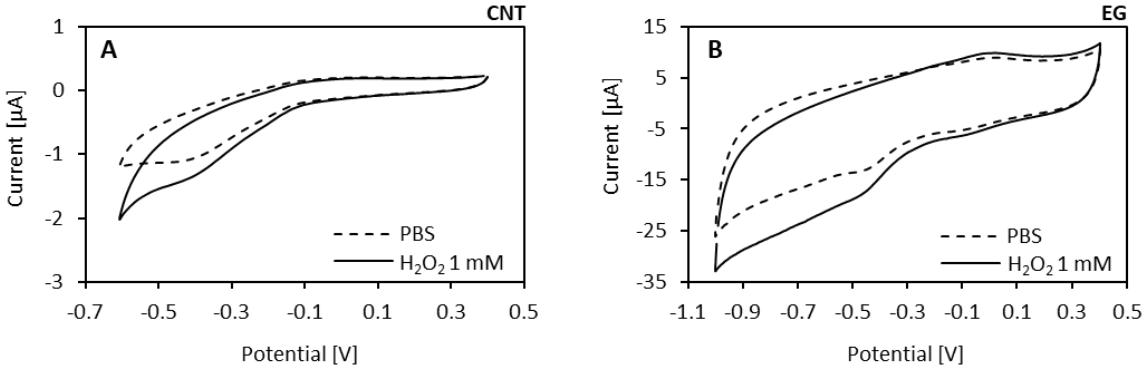

Figure S6. CV responses showing the cathodic currents generated by multiwall carbon nanotubes (A) and exfoliated graphene (B) in presence (solid line) and in absence (dashed line) of 1 mM H_2O_2 (scan rate: 20 mV s^{-1}, electrolyte 0.1 M PBS 0.1 M KCl, WE: GC, CE: Pt mesh RE: Ag/AgCl, Argon atmosphere).

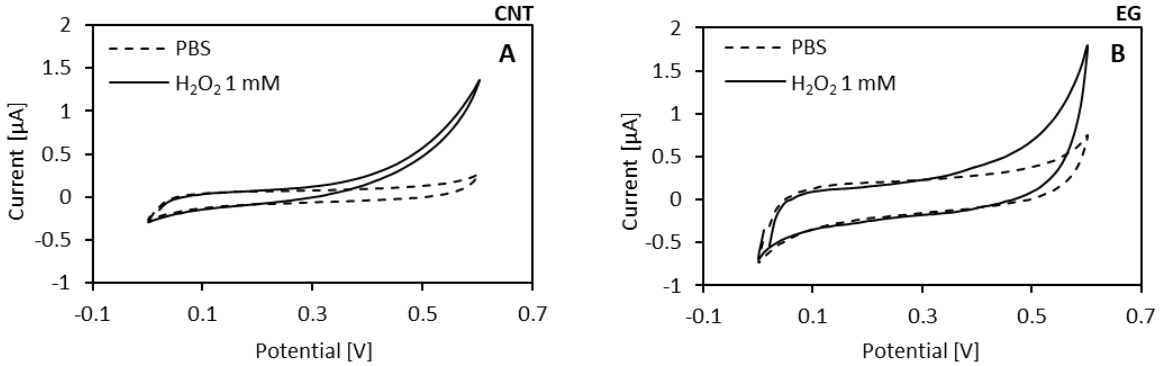

Figure S7. CV responses showing the anodic currents generated by multiwall carbon nanotubes (A) and exfoliated graphene (B) in presence (solid line) and in absence (dashed line) of 1 mM H_2O_2 (scan rate: 20 mV s^{-1}, electrolyte 0.1 M PBS 0.1 M KCl, WE: GC, CE: Pt mesh RE: Ag/AgCl).

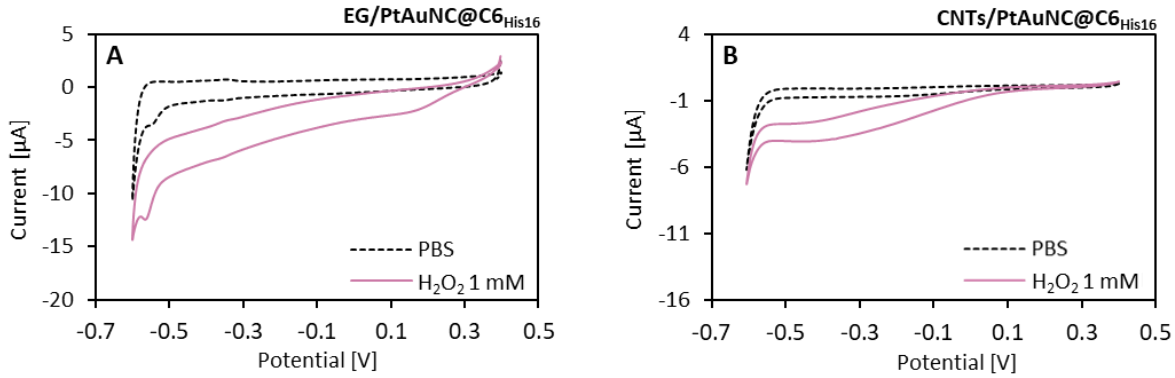

Figure S8. CV responses showing the cathodic currents generated by EG/ PtAuNC@C6$_{His16}$ (A) and CNTs/ PtAuNC@C6$_{His16}$ (B) in presence (solid line) and in absence (dashed line) of 1 mM H_2O_2 (scan rate: 20 mV s^{-1}, electrolyte 0.1 M PBS 0.1 M KCl, WE: GC, CE: Pt mesh RE: Ag/AgCl, Argon atmosphere).

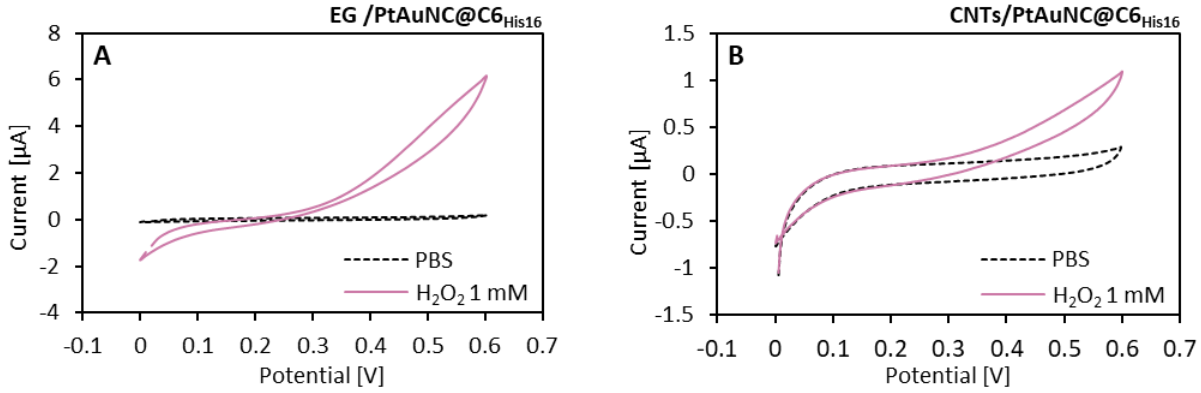

Figure S9. CV responses showing the anodic currents generated by EG/ PtAuNC@C6$_{His16}$ (A) and CNTs/ PtAuNC@C6$_{His16}$ (B) in presence (solid line) and in absence (dashed line) of 1 mM H_2O_2 (scan rate: 20 mV s^{-1}, electrolyte 0.1 M PBS 0.1 M KCl, WE: GC, CE: Pt mesh RE: Ag/AgCl).

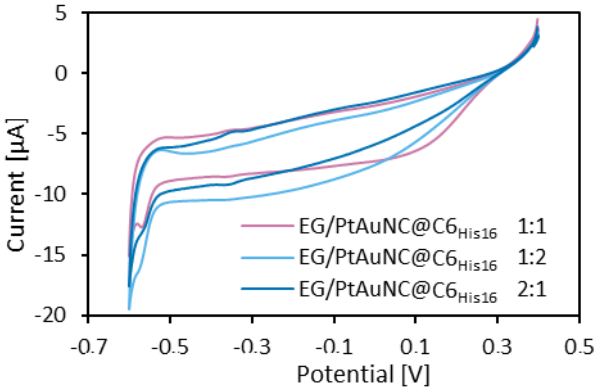

Figure S10. CV responses showing the cathodic currents generated by EG/PtAuNC@C6$_{His16}$ in 1:1 (pink), 1:2 (light blue) and 2:1 (blue) ratio in presence of 1 mM H_2O_2 (scan rate: 20 mV s^{-1}, electrolyte 0.1 M PBS 0.1 M KCl, WE: GC, CE: Pt mesh RE: Ag/AgCl, Argon atmosphere).

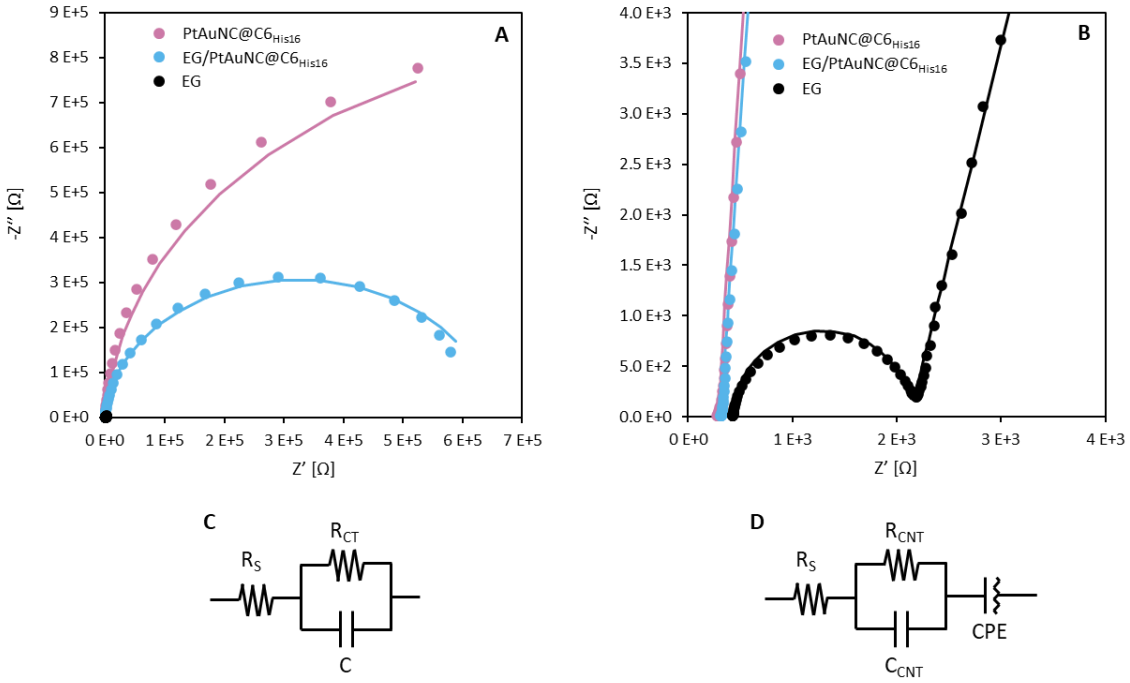

Figure S11. A) Nyquist plots of EG (black), EG/PtAuNC@C6$_{His16}$ (light blue) and PtAuNC@C6$_{His16}$ (pink). The electrochemical impedance spectroscopy was registered in PBS solution (pH=7) containing 1 mM $[Fe(CN)_6]^{3-/4-}$, at the OCP with a perturbation equal to 10 mV in the frequency range comprised between 100 kHz and 10 mHz. B) Magnification of the high frequency region of the Nyquist plot. C) Equivalent circuit for EG/PtAuNC@C6$_{His16}$ and PtAuNC@C6$_{His16}$. D) Equivalent circuit for EG.

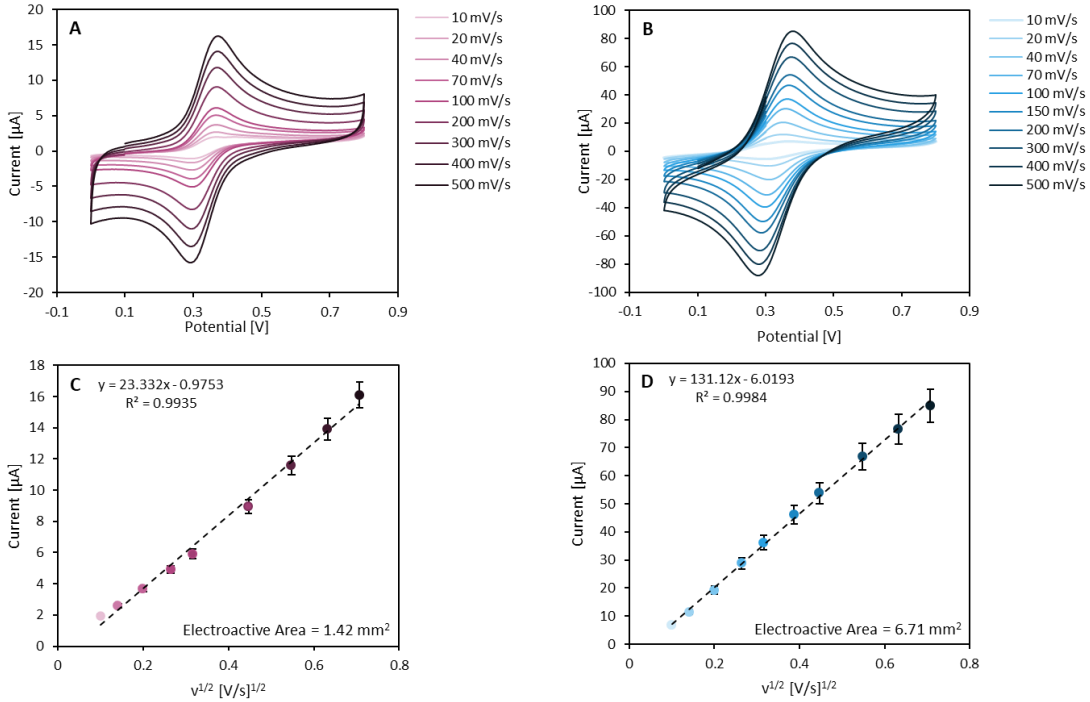

Figure S12. CV responses recorded with GCE in 1 mM Fc-COOH, in 0.1 M PBS and 0.1 M KCl, at increasing potential scan rate, ranging from 10 to 500 mV s^{-1} for PtAuNC@C6$_{His16}$ (A) EG/PtAuNC@C6$_{His16}$ (B). Linear correlation between the anodic peak current and the square root of the scan rate, according to Randles-Sevcik equation, is reported for PtAuNC@C6$_{His16}$ (C) and EG/PtAuNC@C6$_{His16}$ (D).

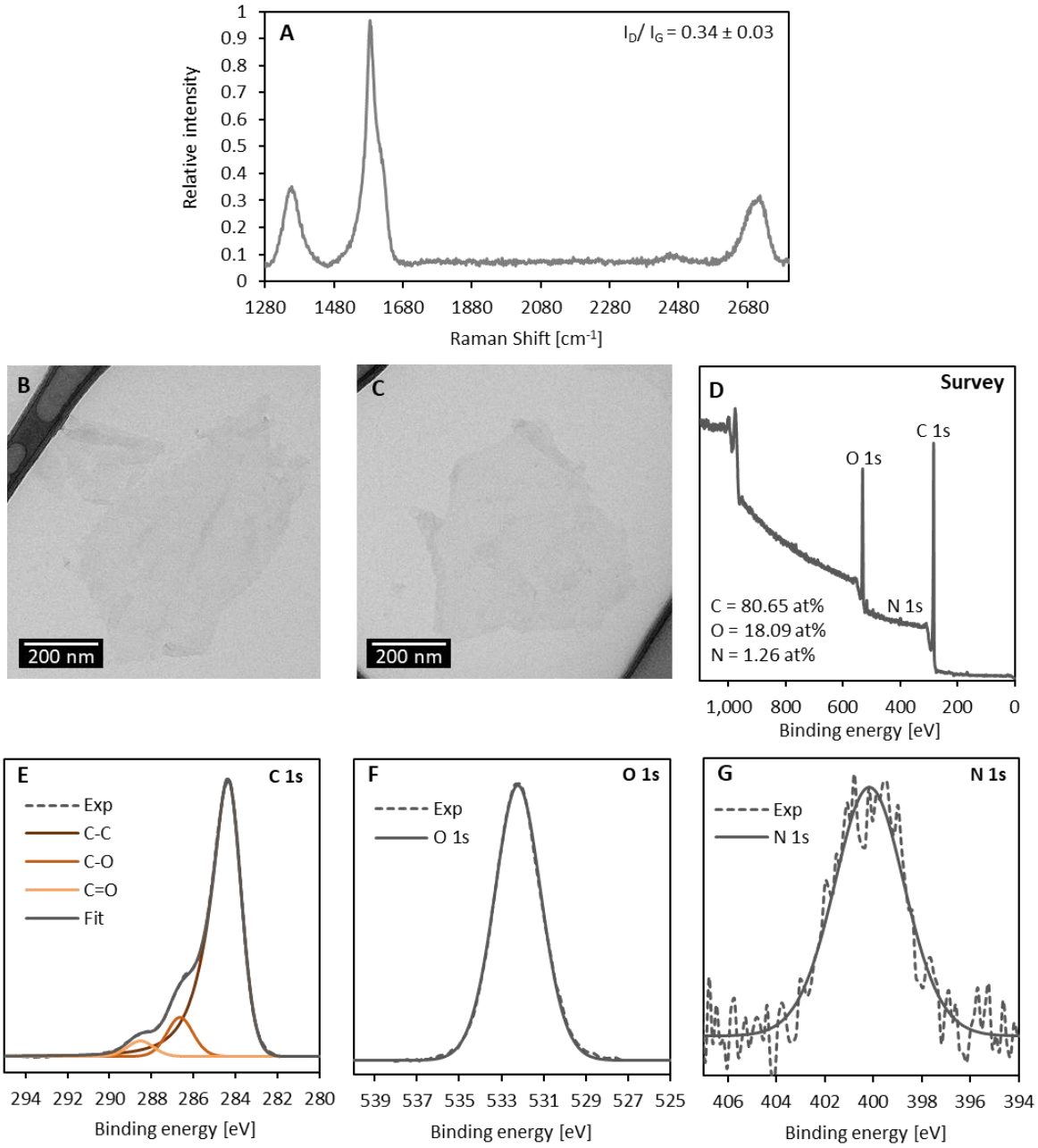

Figure S13. Exfoliated graphene characterization: Raman spectrum (A), TEM micrographs (B, C), XPS survey spectrum (D), deconvoluted high-resolution XPS spectra of the C 1s, O1s and N1s cores (E, F, G).

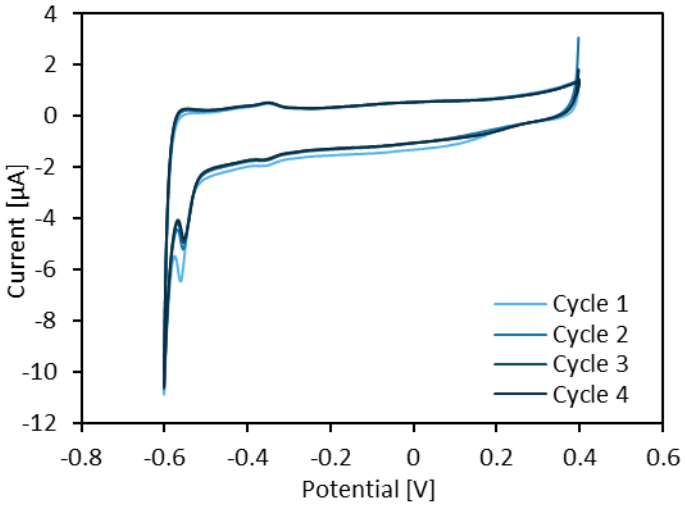

Figure S14. CV traces of EG/AuPtNC@C6$_{His16}$ in presence of 0.1 M PBS + 0.1 M KCl. Four consecutive cycles were registered, with an interval of 20 seconds among them, to test the stability of the material.

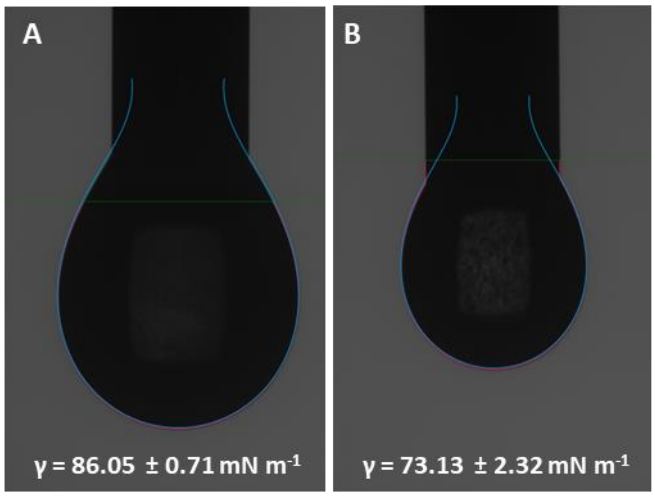

Figure S15. Pendant drop measurements performed to calculate the surface tension of EG/ PtAuNC@C6$_{His16}$ suspended in pure PBS (A) and EG/ PtAuNC@C6$_{His16}$ solution in the full ink formulation (90% PBS, 5% t-butanol, 5% Propylene glycol) (B). The surface tension was calculated applying the Young-Laplace equation.

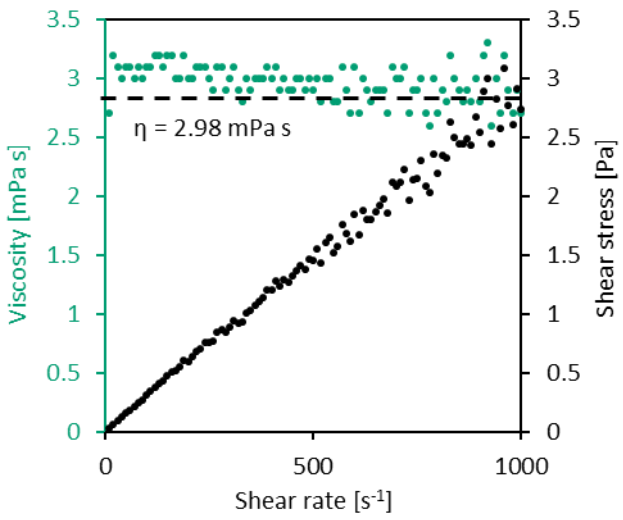

Figure S16. Dynamic viscosity profile of the ink (1 mg ml^{-1}). The viscosity extrapolated at is equal to 2.98 mPa s.

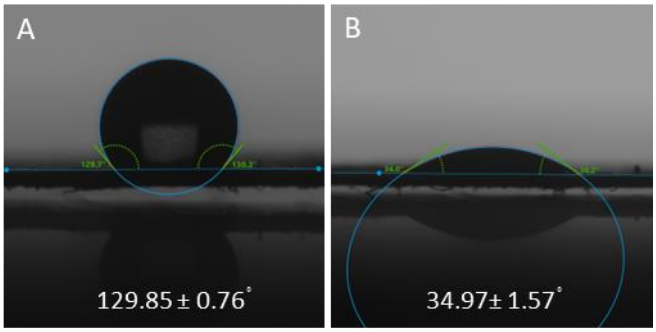

Figure S17. Contact angle measurements of EG/ PtAuNC@$C6_{His16}$ suspended in pure A) PBS and B) EG/ PtAuNC@$C6_{His16}$ solution in the full ink formulation (90% PBS, 5% t-butanol, 5% Propylene glycol) , on partially hydrophobized paper (drop volume 2.0 µL). The ink formulation effectively decreases the surface tension of water in contact with the paper, decresing the contact angle from 129.85° to 34.97° (at timepoint 0.1 s). Furthermore, the ink formulation improves the wettability of the ink allowing complete adsorption within less than 1 second, while the active material in PBS took more than 30 minutes to dry completely.

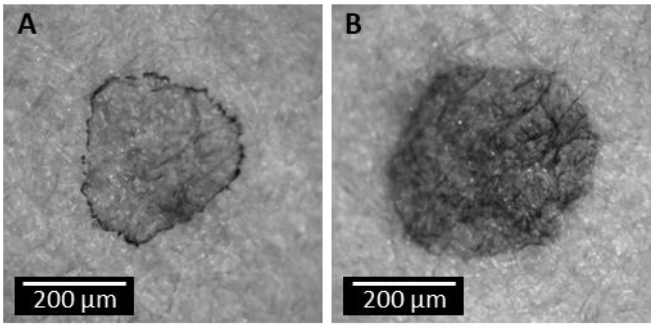

Figure S18. Optical micrographs of the material deposited on partially hydrophobic paper, upon drying a 2.0 µL drop of EG/PtAuNC@$C6_{His16}$ in PBS (A) and the full ink formulation (B). The ink formulation improves the homogeneous distribution of the material in the spot and hinders coffee-ring formation

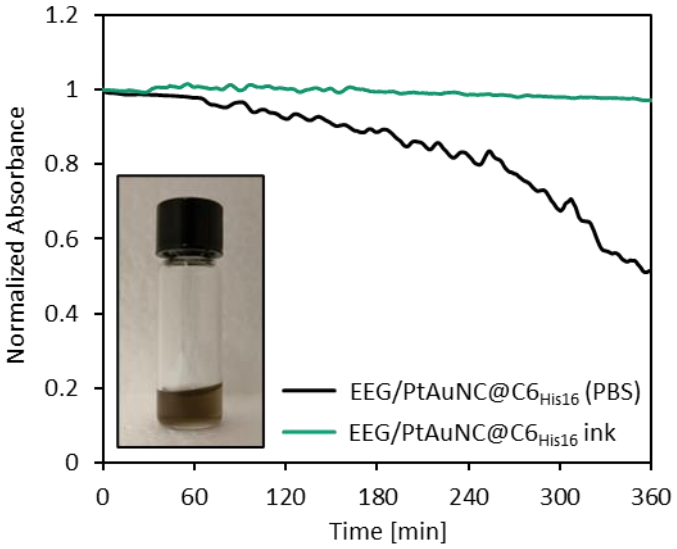

Figure S19. Sedimentation rate of EG/PtAuNC@$C6_{His16}$ (0.25 mg ml^{-1}) ink, evaluated through the variation of the absorption value at 660 nm over the time. The picture in the inset shows the EG/ PtAuNC@$C6_{His16}$ ink at a concentration of 0.2 mg ml^{-1}.

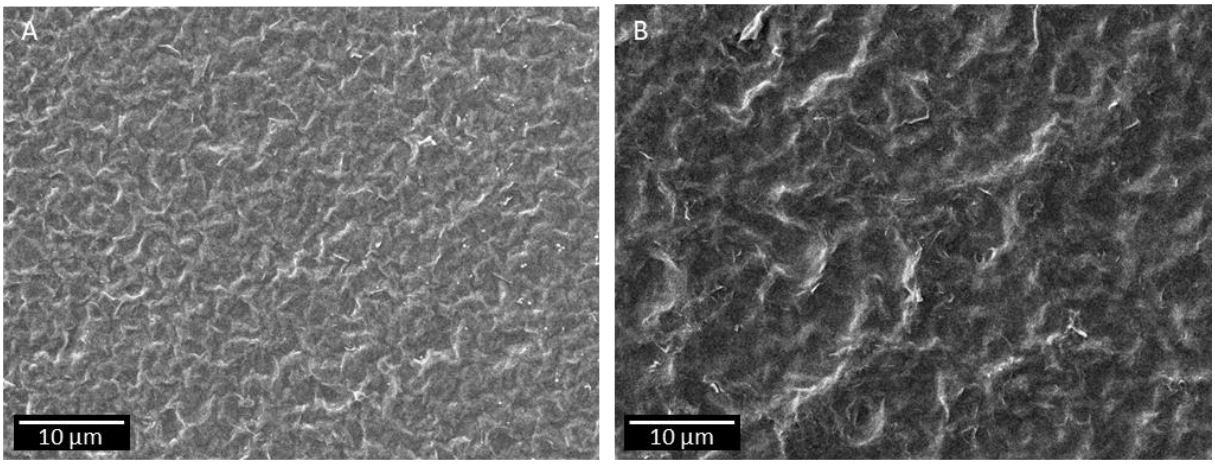

Figure S20. SEM micrographs of the EG/ PtAuNC@C6$_{His16}$ films in presence (A) and absence (B) of 5% t-butanol and 5% propylene glycol.

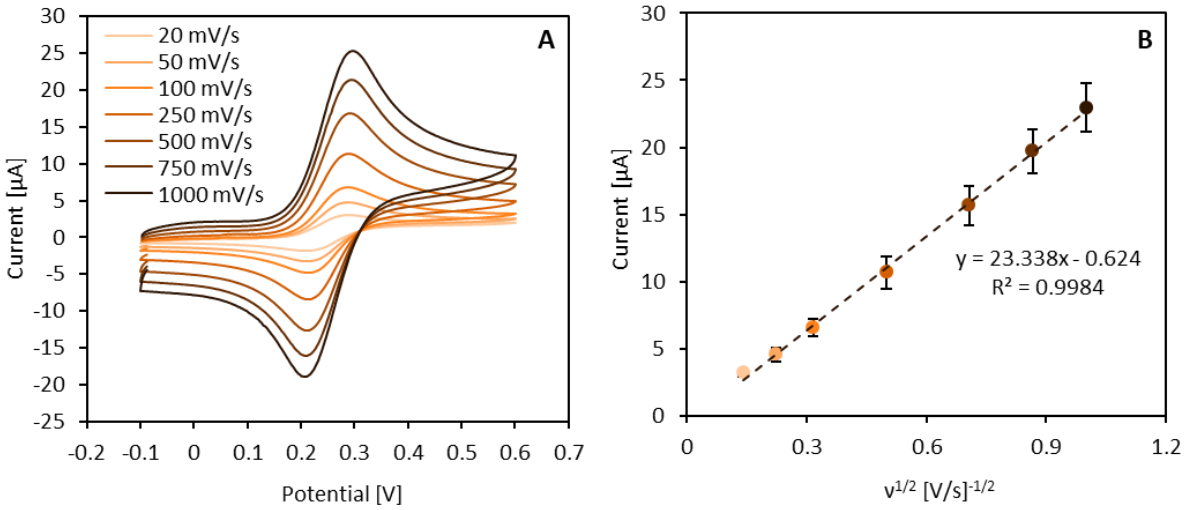

Figure S21. (A) CV responses recorded with IPE in 0.5 mM Fc-COOH, in 0.1 M PBS and 0.1 M KCl, at increasing potential scan rate, ranging from 20 to 1000 mV s^{-1} and (B) the linear correlation between the anodic peak current and the square root of the scan rate, according to Randles-Sevcik equation.

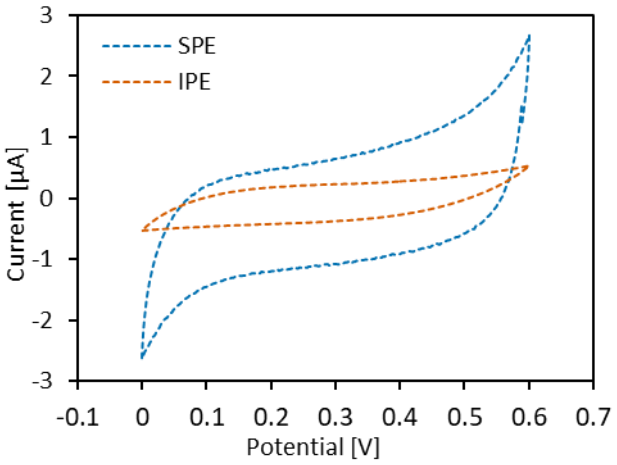

Figure S22. CV responses recorded with IPE and C-SPE in the electrolyte (0.1 M PBS and 0.1 M KCl) showing the capacitive currents for the two systems.

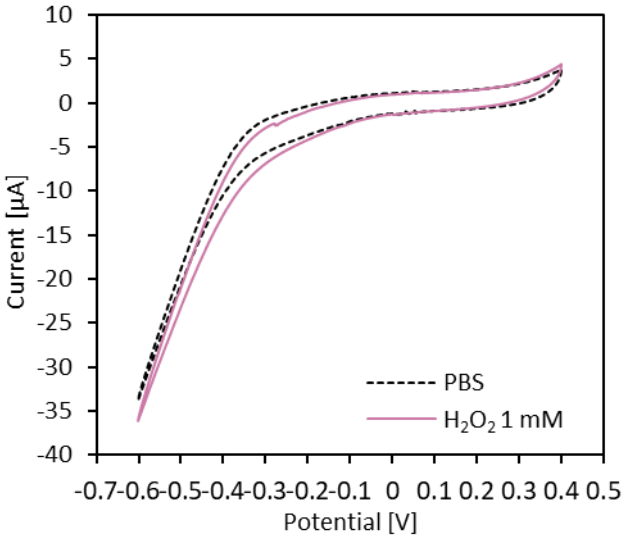

Figure S23. CV responses of IPE modified with EG/ PtAuNC@C6$_{His16}$ in presence (solid line) and in absence (dashed line) of 1 mM H_2O_2, showing a reduced cathodic current in presence of the analyte

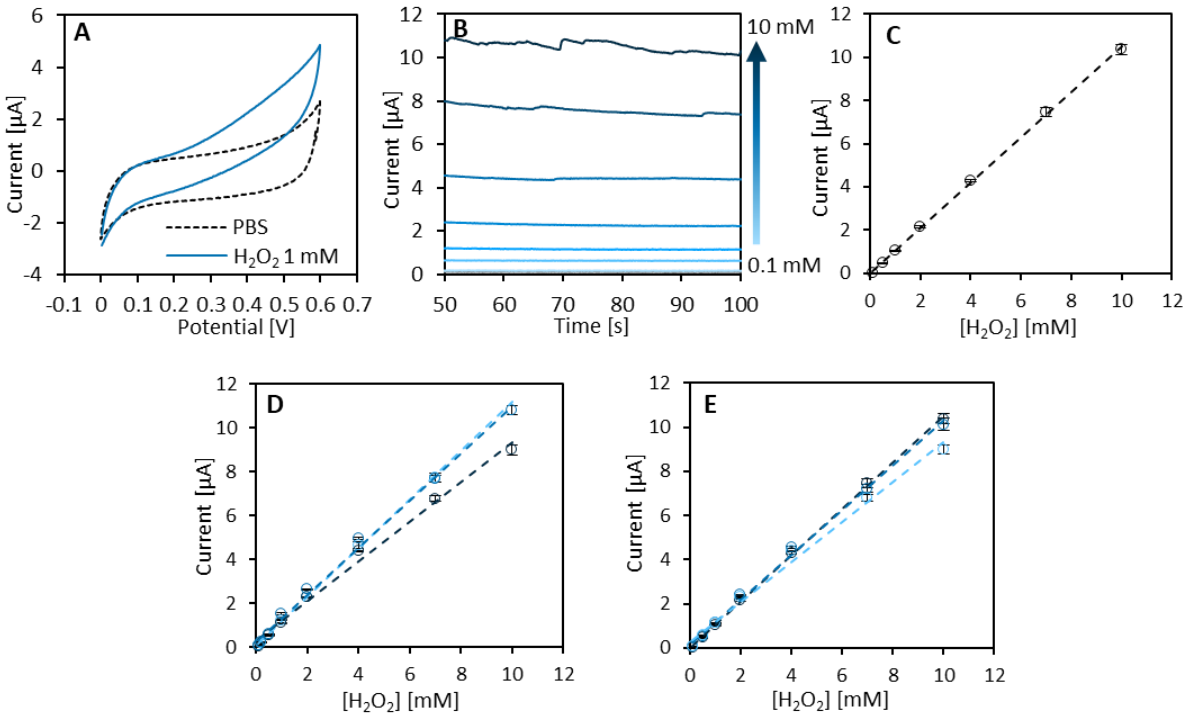

Figure S24. Electrochemical sensing of H_2O_2 concentrations in PBS with C-SPE modified with EG/ PtAuNC@C6$_{His16}$ ink. (A) CV responses obtained with the C-SPE, in the absence (dashed line) and in the presence (solid line) of 1 mM of H_2O_2 (scan rate20 mV s^{-1}). (B) Chronoamperometric response obtained from C-SPE at nine different H_2O_2 concentrations, namely 0.1, 0.2, 0.4, 0.7, 1, 2, 4, 7, 10 mM. (E = +0,4 V). (C) Trend of the current measured in CA vs. H_2O_2 concentrations. The linear regime was found between 0.1 and 10 mM. (E) Calibration lines obtained from three different SPE. The reproducibility RSD% calculated among the three slopes of the linear calibrations was of 10.63 %. (F) Calibration lines obtained from three consecutive CA calibrations on the same SPE. The repeatability RSD% calculated among the three slopes of the linear calibrations was of 7.58 %. Error bars represent the standard deviation during 50 seconds of measurement.

Table S3. Calculation of the price of a IPE

Material	Amount		Concentration		Price/Unit		Price	
Graphene	1.00E-03	ml	1	mg/ml	0.46	€/mg	4.60E-04	€
$PtAuNC@C6_{His16}$	1.00E-03	ml	1	mg/ml	1.03	€/mg	1.03E-03	€
Graphite	4.20E-02	ml	80	mg/ml	6.60E-05	€/mg	2.22E-04	€
Silver ink	1.20E-02	ml	100	mg/ml	7.00E-03	€/mg	8.40E-03	€
Paper	2	cm^2	-		1.71E-04	€/cm^2	3.42E-04	€
Polistyrene	2.00E-01	ml	10%		7.70E-05	€/mg	1.54E-06	€
Electricity	0.083	h	-		1.00E-02	€/h	8.30E-04	€
Electrode price							0.011	€

Table S4. Calculation of the amount of noble metals in the WE

Material	Amount		Concentration		Total amount	
Graphene	1.00E-03	ml	1	mg/ml	4.60E-04	mg
$PtAuNC@C6_{His16}$	1.00E-03	ml	1	mg/ml	1.00E-03	mg
	of which 43% is Au and Pt*				4.30E-04	mg
Graphite	4.20E-02	ml	80	mg/ml	5.04E-01	mg
Percentage of noble metals in the WE					0.08	%